APEM journal
Advances in Production Engineering & Management
Volume 19 | Number 1 | March 2024 | pp 133–148
https://doi.org/10.14743/apem2024.1.498
ISSN 1854-6250
Journal home: apem-journal.org
Original scientific paper

Experimental and numerical investigation of the deep drawing process using a tractrix die – An industrial case study focused on stress and temperature analysis

Mandic, V.[a,*], Milosavljevic, Dj.[b], Jurkovic, Z.[c], Adamovic, D.[a]

[a]Faculty of Engineering of the University of Kragujevac, Kragujevac, Serbia
[b]Sloboda a.d., Cacak, Serbia
[c]Faculty of Engineering of the University of Rijeka, Rijeka, Croatia

ABSTRACT

The deep drawing process of thick sheet metal for vessel production is carried out by applying a tractrix die with the absence of a blank holder, which has economic benefits for industrial production. The main aim of the paper is the development of a reliable numerical thermo-mechanical model of a silicon brass vessel manufactured by a deep drawing process in a tractrix die and a subsequent ironing process, which includes the previous assembly of the dies with reinforcing rings that creates the required prestresses. The testing of the mechanical properties of silicon brass CuZn24Si was carried out by a standard uniaxial tensile test, thus a flow curve was determined to describe the material behaviour. The initial temperatures of the environment, blank and tools were measured with an infrared thermal imager. A comprehensive finite element stress analysis of the deformable tools was carried out for the assembly phase of the dies, and for workpiece and tools in the deep drawing and ironing processes. The comparison of measured and numerically estimated temperatures had a good agreement, so the developed numerical model was confirmed and validated. This research study demonstrates how different process parameters can be investigated through a reliable and precise numerical model with complementary experimental research for the optimization of industrial technology.

ARTICLE INFO

Keywords:
Deep drawing;
Tractrix die;
Reinforcing rings;
Finite element method (FEM);
Experimental-numerical approach;
Numerical modelling;
Simulation;
Infrared imaging technology;
Simufact.forming

**Corresponding author:*
mandic@kg.ac.rs
(Mandic, V.)

Article history:
Received 28 December 2023
Revised 29 February 2024
Accepted 1 March 2024

1. Introduction

Deep drawing is one of the sheet metal forming processes that is widely used in the automotive, aerospace, and packaging industries for the production of parts from various materials. It most often represents the first sheet metal forming operation where a 3D shape is obtained from a relatively flat sheet metal. It is often combined with an ironing operation (DDI – Deep Drawing and Ironing) when, in order to obtain special vessels and liners from thick sheets, it is necessary to maintain an identical thickness at the bottom while significantly reducing the thickness of the vessel walls [1]. In addition to numerous advantages compared to other technologies, it must be noted that the use of this technology is economically feasible only in the case of large-scale and mass production, as it requires the production of special tools as well as the use of machines with

large nominal forces. One of the ways to successfully perform the first deep drawing operation on thick sheets with less forming loads and radial stresses is to use a tool with a tractrix die and without a blank holder [2-3].

Thick sheet forming processes are considered bulk forming rather than sheet metal forming due to large deformations, temperature increase and the appearance of significant radial stresses, where it is necessary to protect the die with reinforcing rings and apply cooling agents. Understanding the influence of numerous process parameters on the stress-deformation-temperature state in the tool and the workpiece during the process is very important for the prevention of defects (wrinkling, folding etc.), excessive radial stresses and obtaining quality workpiece and finished parts [4-6].

There are numerous studies that apply an integrated experimental-numerical approach to the analysis of metal forming processing [7-14] where reliable numerical models have been developed and verified by industrial case studies. The basic condition for a reliable model is the similarity between the real and the model process, which can only be achieved through experimental laboratory tests and measurements in the industrial process. When the conditions of similarity are proven, then a lot of information and results can be obtained from such a validated numerical model of the process about the coupled influence of the process parameters on the output performance, even outside the scope of industrial application, thus the physics of the process itself is explored more deeply.

The purpose of the paper is to develop a reliable numerical thermo-mechanical finite element (FE) model for the analysis of the deep drawing process using a tractrix die, combined with the subsequent ironing process, to obtain a silicon bronze vessel under controlled temperature conditions, in order to achieve the target structure with a significant reduction of the wall thickness. The overall contribution of this study is reflected in the proposed and demonstrated integrated experimental-numerical approach for achieving the conditions of similarity of real and model processes through the experimental identification of process input parameters and model validation. The uniaxial tensile test was used to determine the mechanical properties of silicon brass and the flow curve in mathematical form, to describe the behaviour of the material during plastic forming in FE numerical simulation. To achieve the required contact friction conditions the blank was subjected to mechanical and chemical treatments described in the paper. Using infrared imaging technology, the temperatures of blanks, tools and the environment were measured before and after the industrial process.

2. Deep drawing process using a tractrix die

The profile of the deep drawing die significantly influences the sheet metal flow, the degree of deformation, the change in forming load depending on the puller stroke and, finally, on the quality of the workpiece and the process itself. Three types of the die profiles are used depending on the type of operation, with a transition radius, with a cone and with a specially designed tractrix curve.

When it comes to thick sheets, the die with the tractrix profile gives the best results, especially for consecutive deep drawing and ironing operations in the same tool, such as the case study in this paper. In such a die, the bending arm of the sheet is constant throughout the drawing process. The normal force always acts on the edge surface of the billet creates the largest bending arm. Considering that the arm h moves along the tractrix curve tangentially, the solution boils down to finding the equation of the tractrix curve with constant tangent length. Fig. 1 shows the profile of the die with the tractrix curve in the Cartesian coordinate system, and the Eq. 1 defines the tractrix curve with a constant tangent length [15]:

$$x = h \cdot l_n\left(\frac{h+\sqrt{h^2-y^2}}{y}\right) - \sqrt{h^2 - y^2} \tag{1}$$

The weakness of the tractrix profile is that it theoretically has an infinite height ($\lim_{y\to 0} x \to \infty$), so it is necessary to adjust the initial value h_0, so that the deep drawing does not start at the very end of the tractrix curve but moves closer to the x axis. It is recommended that h_0 be slightly larger than the radius r_m for the drawing die with a radius. For the recommended value of the height of the tractrix curve in the die profile, it is necessary to choose the appropriate value of y_0.

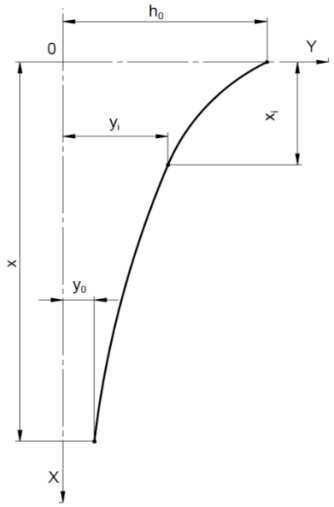

Fig. 1 Die profile with a tractrix curve

Taking into account the billet dimensions used in the industrial case study for the purposes of this paper ϕ 227 × 15 mm, and the outer diameter after deep drawing ϕ 163.5 mm, the value h_0 = 30 mm was chosen, so that Eq. 1 has the form:

$$x = 30 \cdot l_n\left(\frac{30+\sqrt{30^2-y^2}}{y}\right) - \sqrt{30^2 - y^2} \tag{2}$$

Pairs of values (x, y) for the tractrix profile of the die are shown in Table 1, and the technical drawing of the die is shown in Fig. 2.

Table 1 The coordinates of the points belonging to the tractrix profile

Point	1	2	3	4	5	6	7	8	9	10	11
Y (mm)	30	28	25	22	19	16	13	10	8	6	4
X (mm)	0	0.488	2.064	4.438	7.643	11.82	17.27	24.53	30.92	39.299	51.284

3. Methods and materials

3.1 Integrative experimental-numerical approach

For the analysis of the deep drawing process, an integrative approach that includes experimental and numerical methods was applied, as a proven way to prepare high-quality input data and boundary conditions for the application of the finite element method and its verification, schematically shown in Fig. 3. In this approach, the process must be observed as a system of interconnected relevant parameters that include the following subsystems:

- *Billet:* size and shape, material, chemical composition and microstructure, flow properties under processing conditions (flow stress as a function of deformation, deformation rate and temperature), thermal and physical properties;
- *Tool:* geometry, surface condition, material and hardness, temperature, stiffness and accuracy;
- *Interface conditions:* finalization of surfaces, lubrication, friction and heat transfer;
- *Deformation zone:* mechanics of plastic deformation, material flow, strains, stresses, strain rates and temperatures;
- *Production equipment:* machine type, velocity, maximum load / available energy, stiffness and precision.

Numerical process modelling, supported by experimental data and tests, is used to predict material flow, determine distributions of strains, stresses, temperatures, tool stresses, potential sources of defects and brittle fracture, properties and microstructure of workpiece, as well as assessment of elastic springback and residual stresses.

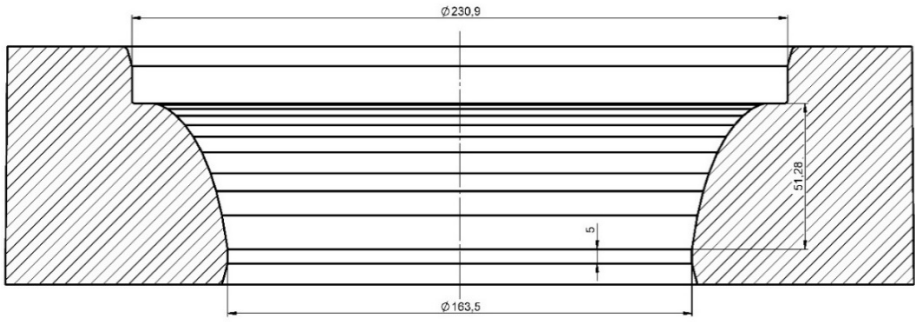

Fig. 2 Technical drawing of the die with a tractrix profile

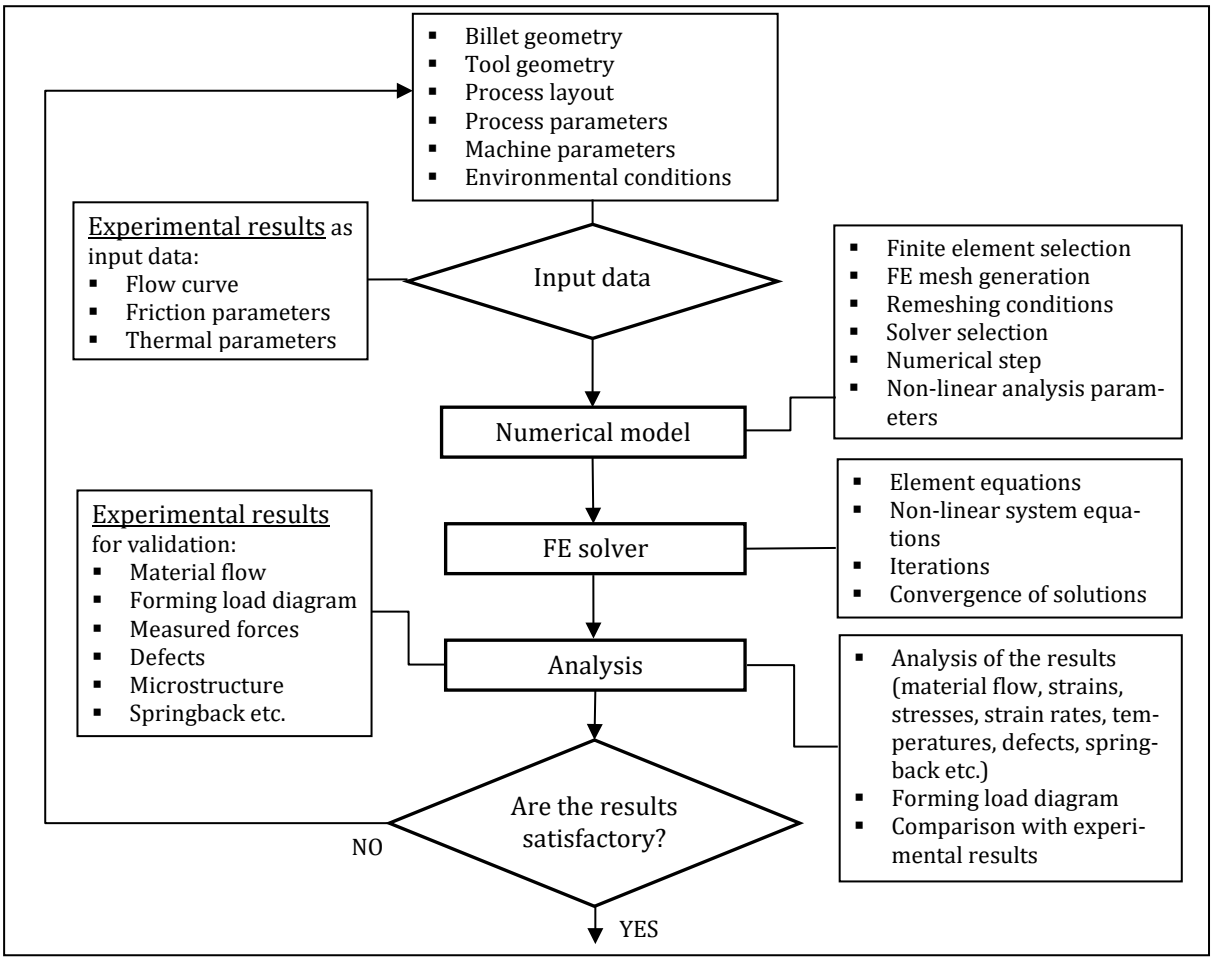

Fig. 3 Integrative experimental-numerical approach in process modelling

For the results of numerical modelling to be reliable, it is necessary to provide high-quality input data that faithfully describe the real industrial process and refer to the geometry of applied tools and billet, and process and environmental parameters. In addition, it is necessary to perform experimental research to determine the true stress – true strain relationship (flow curve) for the materials of the billet and the tool, if the tool stress analysis is taken into account. The conditions of contact friction, heat transfer and radiation are described by appropriate laws for which it is necessary to experimentally determine the friction coefficient/factor, heat transfer coefficient and emissivity coefficient.

In the pre-processing phase a numerical model of the process is developed, using all input data and through the selection of the appropriate finite element, defining the conditions for generating the initial FE mesh, as well as the subsequent remeshing, the selection of the appropriate solver, the number of numerical steps and other parameters for non-linear FE analyses. If all previous

steps are well defined, the FE calculation itself is realized automatically by means of the solver by iteratively solving the nonlinear equations of the system with the convergence of the solution.

The selection of numerical results for the analysis depends on the goals of the process simulation, but those that can be compared with the experimental ones should be chosen, in order to verify the numerical model of the process. For this purpose, laboratory or industrial experiments can be carried out. When the comparative analysis of the results shows an unsatisfactory match or the obtained results are not as expected by the set goals, it is necessary to repeat the simulation with changed input parameters and settings for FE analysis.

3.2 Material properties

One part of the experimental research was related to the characterization of the workpiece material and the determination of flow curves using the uniaxial tension test. The tested material was silicon brass (Plate EN 1652 – CuZn24Si – R500) containing 23.13 % Zn, whose complete chemical composition is given in Table 2.

Table 2 Chemical composition of silicon brass CuZn24Si

Element	Cu	Pb	Fe	Sn	A_l	Ni	P	Si
%	75.9	0.004	0.002	0.007	0.003	0.003	0.006	0.940

This chemical composition of brass is suitable for deep drawing of thick sheets (in this case 15 mm) considering the higher percentage of Zn gives better material ductility. The presence of silicon results in an increase in resistance to general and stress corrosion, and, in addition, it has a very favourable effect on the mechanical properties of brass, both at room and elevated temperatures. Previous research on this silicon brass have shown that the best technological properties are obtained if silicon is added to brass with a stoichiometric composition of Cu_3Zn, i.e. to brass with 75 % of Cu, as well as with the addition of silicon over 0.5 % [16]. However, higher percentages of silicon can negatively affect the formability of the material.

Uniaxial tensile tests were performed on a Zwick/Roell Z100 universal material testing machine, which enables automatic data acquisition at a speed of 500Hz. A ceramic extensometer in the range of 11-50 mm was used to measure elongation. The strain, strain at break, yield strength and tensile strength values were calculated using testXpert software and the collected pairs of load and elongation values. A total of 9 specimens were prepared, three for each of the rolling directions (0°, 45° and 90°), due to the reproducibility of the obtained results, and according to the standard ISO 6892-1:2019, with original diameter of 8 mm and original gauge length of 100 mm. Specimens after one series of tests are shown in Fig. 4. Holloman's hardening law given by Eq. 3 was used for the mathematical formulation of the material's behaviour during deformation:

$$k_f = C\ \varphi^n, \text{MPa} \tag{3}$$

where k_f is flow stress, C is strength coefficient, φ is true strain, and n is hardening exponent. The obtained mechanical properties of the material are shown in Table 3, as average values for three repeated tests.

Fig. 4 Specimens after uniaxial tension test

Table 3 Mechanical properties of CuZn24Si brass

Rolling direction	Stress (MPa)		Strain		Coefficients in Eq. 3	
	Yield stress	Ultimate stress	Strain (ultimate)	Strain at break	C	n
0°	94.63	558.04	0.5288	0.5647	779.69	0.52886
45°	94.10	552.96	0.5300	0.5683	768.63	0.52591
90°	92.11	554.01	0.5259	0.5540	768.29	0.53004

3.3 Numerical modelling

The application of numerical process modeling is a well-proven and extremely useful tool for predicting problems in industrial production and reducing time and cost in new product development. For metal forming modeling based on the finite element method, it is necessary to apply a nonlinear coupled thermo-mechanical approach, since due to plastic deformation and the influence of contact friction, there is an increase in temperature in the workpiece. In order to realistically describe industrial process, modelling must include, in addition to heat generation in the workpiece, the heat transfer to the tool and its radiation to the environment. Although the considered deep-drawing process takes place at room temperature, due to the bulk forming of the thick sheet, this process can be considered a bulk forming process, in which the temperature in the workpiece can rise by several hundred degrees. Due to all of the above, only a coupled finite element approach can provide reliable numerical modelling results.

In this study, the *Simufact.forming* software was applied as a virtual manufacturing tool, which applies the enhanced version of the *MARC* finite element solver based on the displacement method and the coupled thermal-mechanical approach [17]. The constitutive relations for this approach are defined by Eqs. 4 and 5:

$$K(T) \cdot u = f \tag{4}$$

$$C(T) \cdot \dot{T} + k(T) \cdot T = Q + Q^1 \tag{5}$$

where K is the system stiffness matrix, u is the nodal displacement, f is the force vector, C is the heat capacity matrix, T is the nodal temperature vector, $\dot{T}$ is the time derivative of the temperature, k is thermal-conductivity matrix, Q is the thermal load vector (flux) and Q^1 is the internal heat generated due to plastic deformation. K, k and C are all temperature dependant.

The nodal force vector f in Eq. 4 includes the sum of different types of loads:

$$f = f_{point} + f_{surface} + f_{body} + f^* \tag{6}$$

where f_{point} is the point load vector, $f_{surface}$ is the surface load vector, f_{body} is the volume load vector, and f^* represents all other types of load vectors (for example thermal strains).

In metal forming processes, these equations are non-linear due to the non-linearity of the material and geometry during deformation, as well as due to the constant changes in boundary conditions (contact friction and thermodynamic processes). To solve them, a Newton-Raphson incremental method is used, within the iterative solver. A direct solver can also be used, but it requires more processing time, but offering more accurate solutions.

To establish a connection between the real 3D stress state existing in the workpiece during deformation and the flow curves obtained by the uniaxial tensile test, the Von Mises flow function, usually for plastic materials, is used. According to this criterion, plastic flow of the material occurs when the calculated effective stress reaches the yield strength determined by the tensile test. When it is necessary to include material anisotropy into the modelling process, which is especially significant in thin sheet metals, this software uses the Hill anisotropic yield function.

In a coupled thermo-mechanical numerical approach, the critical input parameters for numerical modelling are mechanical and heat properties of workpiece and tools, material model that includes an elastic-plastic behaviour with strain hardening, initial temperatures, heat transfer and emissivity parameters as well as friction properties for the interface.

No less important is the choice of the appropriate finite element that enables obtaining convergent solutions in the calculation, then automatic generation of the initial FE mesh in the workpiece and tool, and automatic remeshing according to trigger criteria and conditions for mapping parameter values from the old to the new FE mesh. Shell elements are usually used for modelling the sheet forming process, but in the case of thick sheet metal, they do not give satisfactory results. Therefore, in this study, 3D solid isoparametric eight-node hexahedral elements were applied, with automatic detection of sheet thickness and determination of the optimal number of elements through the thickness and the best in-plane element size.

When modelling multistage processes, the virtual manufacturing software should "remember" the entire history of deformation through which the workpiece is transformed, whether the first

stage is related to heating or not, followed by the transfer of workpiece to the tool, in which the workpiece is formed through a series of successive different forming operations, and sometimes interoperational thermal treatments. At the end of forming, the workpiece removal from the tool, the release of elastic strains (springback) should be modelled. During the numerical setup of the process, it is necessary to precisely define the complex kinematics of metal forming machines, because the choice and change of the machine significantly affects the material flow. The applied software for numerical modelling in this study enables all the mentioned requirements.

3.4 Infrared thermal imaging

Infrared thermography is one of the non-contact methods of temperature measurement that is increasingly used for scientific and industrial measurements of temperature fields, especially when contact methods are limited by accessibility or the range of high temperatures in technological processes. This is of particular importance for metal forming processes, because by measuring temperatures in the visible part of the workpiece and the tool itself, places with critical temperature stresses can be identified. When measurements are used to set boundary conditions in numerical modelling or to validate numerical process models, then such an experimental-numerical approach opens up possibilities for numerical estimations of temperature fields outside the experimental range, for example in hot forging processes [18], extrusion at high velocities and industrial ironing processes.

Non-contact methods of temperature measurement are based on the principle of measuring the energy of electromagnetic radiation emitted by the measured object. Infrared radiation is located in the electromagnetic spectrum between visible light and microwave radiation in the range of wavelengths from 0.75 μm to 1 mm. The main advantage of infrared thermography, compared to other methods of temperature measurement, is that a visual image of the temperature field is obtained, where points with maximum or minimum temperature values, as well as their arrangement and mutual dependence, can easily be seen.

Within the thermal interaction of the measured object with the environment, the total energy emitted from the environment is divided into absorbed, reflected and transmitted energy. For measuring the temperature of solid bodies that are impervious to thermal radiation, only the energy emitted by the body is relevant, and it is equal to the absorbed energy. The characteristic by which the radiation of any body is compared with the radiation of a black body is called emissivity expressed through the emission coefficient ε. All bodies have an emissivity greater than 0 (ideal mirror) and less than 1 (black body). The emission coefficient of an object depends on the type of material and the state of the object's surface. For precise measurement of objects made of materials with low emissivity, clean and polished metals with shiny surfaces, emissivity correction is necessary, precisely through the emission coefficient. Before measuring, it is necessary to adjust the emissivity settings in the imager in order to accurately calculate the temperature of the measured object [19].

To calculate the object's temperature, the Stephen–Boltzmann law is applied, which exhibits the relationship between the radiation energy and the temperature by the Eq. 7 [20]:

$$E = \varepsilon \cdot \sigma \cdot T^4 \tag{7}$$

where E is the radiant power of the object; ε is emissivity of material; σ is the Stephen–Boltzmann constant; T is the absolute temperature of the object.

Fluke Ti400 Infrared Thermal Imager and accompanying *SmartView* software were used for experimental measurement of temperature fields in the workpiece and deep drawing tools in this study [21]. The change in emissivity for different materials and conditions of the surface of the object can be changed directly by entering the desired value or using coefficients from the software database. The imager uses manual focusing mode or automatic focusing through the *LaserSharp* system that measures the distance of the object with a laser and the system adjusts the focus for thermal imaging processing. *SmartView* enables the analysis and processing of obtained thermal images for comparative analysis with numerically estimated temperature fields.

4. Industrial case study

4.1 Deep drawing industrial setup

The tool for industrial experiments of the deep drawing process was manufactured by the Sloboda company and mounted on a hydraulic press with a selected deformation speed of 50 mm/s. Fig. 5 shows the technical drawing of the tool assembly. The tool consists of the following components: 1) puller, 2) upper die, 3) intermediate plate, 4) lower die, 5) remover and 6) base plate.

The puller (1), made of alloyed cold-work tool steels 1.2379/X153CrMoV12 (EN ISO 4957:2000) and heat-treated to a hardness of 60HRc, participates in forming the inner shape of the drawn vessel. It has a good ratio of high outer surface hardness and high core durability. The surface of the working part of the puller is polished to the quality of surface treatment N4. In the upper die (2), the workpiece is drawn from the billet into vessel, with a smaller reduction in wall thickness. The material for the upper die is the same as for the puller and lower die. In the lower die (4), the ironing process is carried out to obtain the final shape of the vessel, the thickness and the height of the walls.

Both dies were reinforced with reinforcing rings of 1.7225/42CrMo4 tempering steel (DIN EN 10088) with a 1 mm overlap to achieve prestressing of the dies. Assembly of the rings on the dies was realised by pressing on the press. The dies strengthened in this way are finally mounted in the lower tool holder, as shown in Fig. 6.

4.2 Blank preparation

The circular blank (ϕ 227 mm) was prepared by cutting with a high-pressure water jet from a brass plate of 15 mm thickness (Fig. 7). After cutting, the blank was subjected to strict dimensional and visual control, as well as metallographic examination of the micro and macrostructure. A chemical treatment was applied by immersing the blank in a 10 % solution of sulfuric acid (H_2SO_4) at a temperature of 60-70 °C for 5 minutes. Then the blank was immersed in a 5 % solution of soap emulsion at a temperature of 60 °C. With these procedures, a better plastic flow of the material, a reduction in the impact of contact friction and less heating of the tool were achieved.

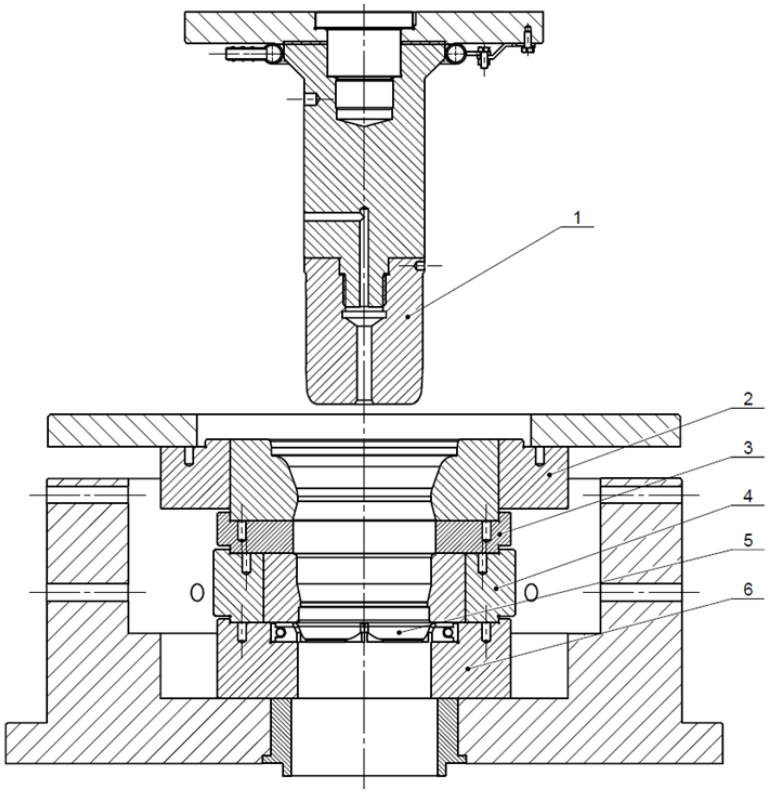

Fig. 5 Technical drawing of the tool assembly

a) b) c)

Fig. 6 Assembly of the lower deep drawing tool with reinforcing rings: a) lower die b) upper die c) assembly

Fig. 7 Cutting the blank by the water-jet process (left) and the blank after chemical treatments (right)

4.3 Measuring the initial temperatures in industrial experiments

In thermo-mechanical FE analysis using the finite element method, it is crucial to provide high-quality and reliable input data, not only for plastic flow of materials, but also for thermodynamic processes. *Fluke Ti400 Infrared Thermal Imager* was used to measure the temperatures of the blank, the environment and the tool in the industrial process, with prior adjustment of the emissivity coefficient. The initial temperature of the blank was 20.7°C, the tool 18.2°C and the environment 18.8°C. However, as the blank before deep drawing was immersed in a heated soap emulsion, in order to reduce contact friction during the process, the measured temperature of the blank placed in the tool was 30.7°C. Fig. 8 shows the registered temperatures.

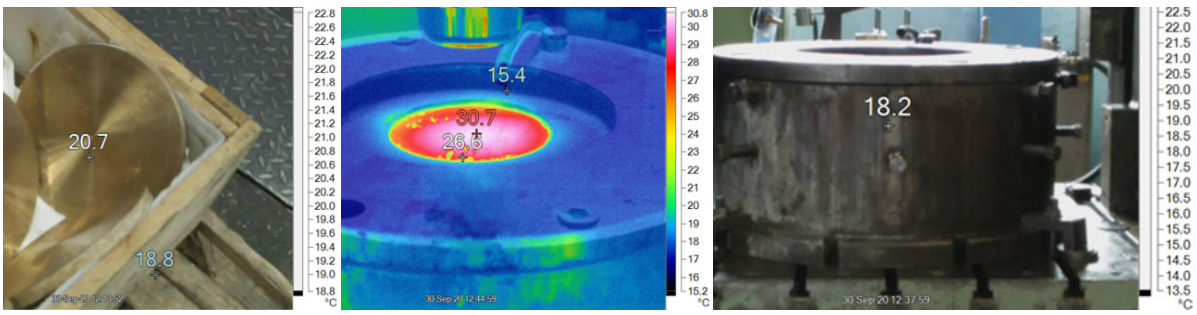

Fig. 8 Initial temperatures in industrial process (blank before and after soap emulsion, environment and tool)

4.4 Numerical model setup

The numerical model of the deep drawing process was set according to identical conditions in the industrial experiment using *Simufact.forming* software and its solver based on the finite element method. *3D CAD* models of tool components in *IGES* format were applied, the assembly of which is shown in Fig. 5. The geometry of the reinforcing rings is simplified, and instead of the intermediate plate, the boundary conditions for fixing the nodes along the horizontal plane in the direction of the *y* axis were defined. Given that it is necessary to achieve absolute similarity between the

industrial and numerical process model, firstly related to the assembly of the upper and lower dies and their reinforcement with rings, the numerical model first included simulations of reinforcing and prestressing of the upper and lower dies. Then, the prestressed tools with deformation history were used for a coupled simulation of the deep drawing process, where the stress, strain and temperature fields in the workpiece and in the tools were monitored simultaneously.

The simulation of the prestressing of the dies by the reinforcing rings was carried out with a virtual overlap of 1 mm as one of the boundary conditions, while other contact conditions between the tool components and blank were defined using the *Contact table*. Instead of the properties and flow curves of the tool steel from which the die and ring were made, materials from the *Simufact material database* used for heat-treated tool steels were applied, for the die material HM560 and for the ring material ASP. The dies and rings were considered deformable while the base plate was considered rigid. The contact friction conditions between the dies and the rings were defined as dry with a friction coefficient of 0.4. Since the process is axisymmetric, a 2D numerical analysis was applied. A *Quadtree* mesh of two-dimensional finite elements with an element size of 1 mm was created on deformable tools.

For the numerical simulation of the deep drawing process, a cylindrical blank with identical dimensions as in the industrial process was modelled, on which a *Quadtree* mesh of two-dimensional finite elements with an element size of 1.3 mm was prepared. Due to significant deformations of the material in the areas of the calibrating bands in both dies, and thus greater distortion of the FE mesh, two refinement boxes were defined in which the number of FE elements was doubled during the simulation and the mesh was regenerated automatically (Fig. 9a).

The material behaviour was described by the flow curve according to Eq. 3 with coefficients' values C=779.69 and n=0.52886, for rolling direction 0°. The workpiece does not represent a finished part, so it was not necessary to take into consideration the anisotropy of the material when analysing the stresses and temperatures in the workpiece and the tool in the axisymmetric process. For the forming process, the contact friction conditions were described by Coulomb's law, where the given value of the friction coefficient was 0.12. The initial temperatures of the tool components, the blank and the environment were as registered and described in the previous section. The working stroke of the press was set at 300 mm. The numerical model of the deep drawing process is shown in Fig. 9b.

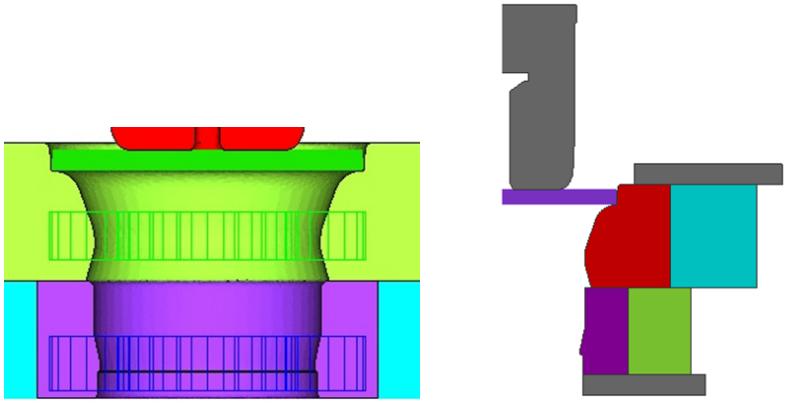

a) b)

Fig. 9 Position of the refinement boxes (a) and 2D numerical model of the deep drawing process (b)

5. Results and discussion

Within this section, the results of all three numerical simulations are presented, both the assembly and prestressing of the upper and lower dies, as well as the coupled simulation of the deep drawing process with deformable tools. The analysis and discussion of the results will focus on stress fields in the workpiece and tools during the process and after workpiece release. Finally, a comparative analysis of measured temperatures in the industrial process and numerically estimated temperature fields in the workpiece and the tools will be presented and discussed.

The radial stress distributions obtained in the simulations of mounting the reinforcing rings on the upper and lower dies, with a virtual overlap of 1 mm, are shown in Fig. 10. It is noticeable that the maximum compressive radial stress in the upper die is -385 MPa and in the lower die -639 MPa. The fields of maximum stresses are located in the overlapping zones of the dies and the rings and mainly in the central part of the dies. The obtained prestress values in the upper die are lower than recommended (600-700 MPa), which is caused by the small value of the total overlap of 1 mm in relation to the outer diameter of the matrix of ϕ 330 mm.

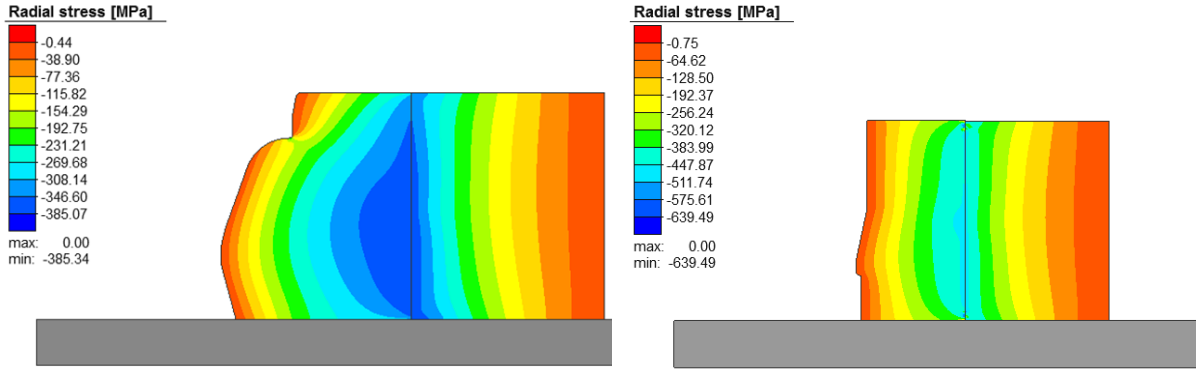

a) b)

Fig. 10 Radial stress distribution of the reinforced upper die (a), lower die (b) in the assembly phase (1 mm overlap)

The recommendation for the overlap value, when installing reinforcing ring, is 0.1 mm for every 25 mm of a diameter. For the lower die, the overlap is adequate considering that the outer diameter of is ϕ 240 mm, so the obtained prestress is approximately the same as the recommended one. For the upper die, it is necessary to implement the overlap of 1.32 mm. Therefore, another simulation of the reinforcing upper die with a new value of the virtual overlap was performed. Fig. 11 shows the distribution of radial stresses in the upper die and ring with a larger overlap, where higher maximum values of radial stresses were obtained in the amount of 587 MPa. In this way, the optimal values of die reinforcement and prestressing can be determined by tool assembly finite element numerical simulation. Arbitrarily chosen values of the overlap between the ring and the die and thus the prestresses can have negative consequences on the tool life, as well as on the dimensional accuracy of the workpiece.

Simufact.forming software allows the transfer of deformation history from operation to operation. Thus, the strain and stress fields in the deformable tools (upper and lower dies and both rings) from the previous simulations of the reinforcing dies were imported into the next simulation of the deep drawing process. In this numerical simulation, the approach of simultaneous complete FE analysis of workpiece forming and elastic deformation in deformable tools was applied. Only in this way reliable results comparable to the industrial process can be obtained.

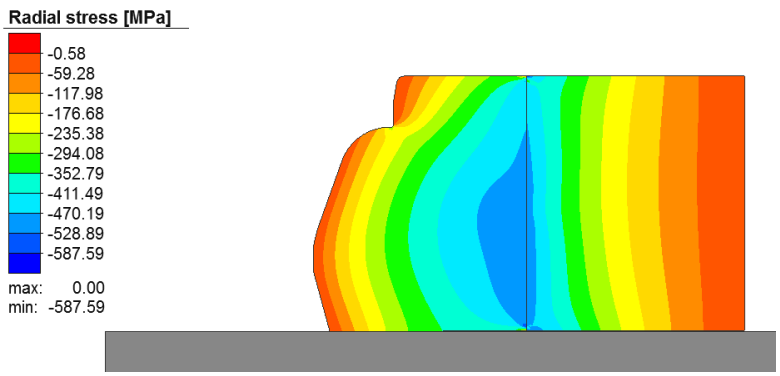

Fig. 11 Radial stress distribution of the reinforced upper die (1.32 mm overlap)

Fig. 12 shows the radial stress distributions in the workpiece and tools in the selected stages of the process. The first stage shown at 19.5 % of the puller stroke was chosen because there is a maximum contact zone between the workpiece and the tractrix profile of the upper die. It is evident that the compressive radial stresses in the upper die have decreased to the value of -400 MPa and the appearance of smaller tensile radial stresses up to 100 MPa (Fig. 12a). The state of the radial stresses in the lower die is almost unchanged. In the workpiece, maximum tensile radial stress was at the bottom of the vessel, the values of which range from 200-280 MPa.

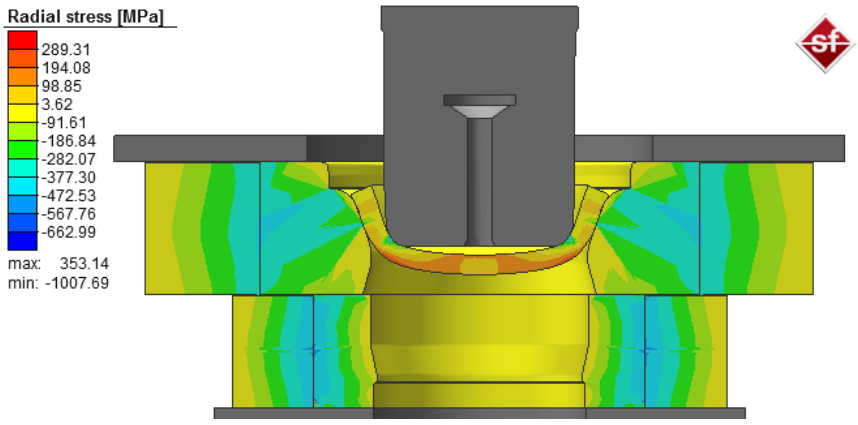

a) 19.5 % of the puller stroke

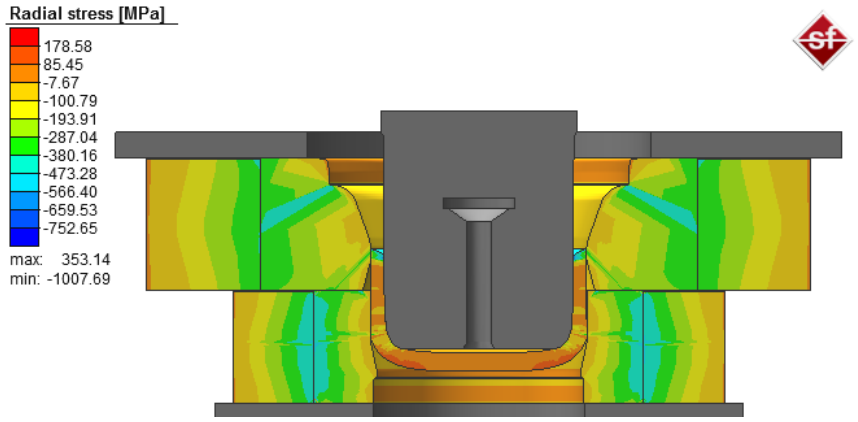

b) 46.4 % of the puller stroke

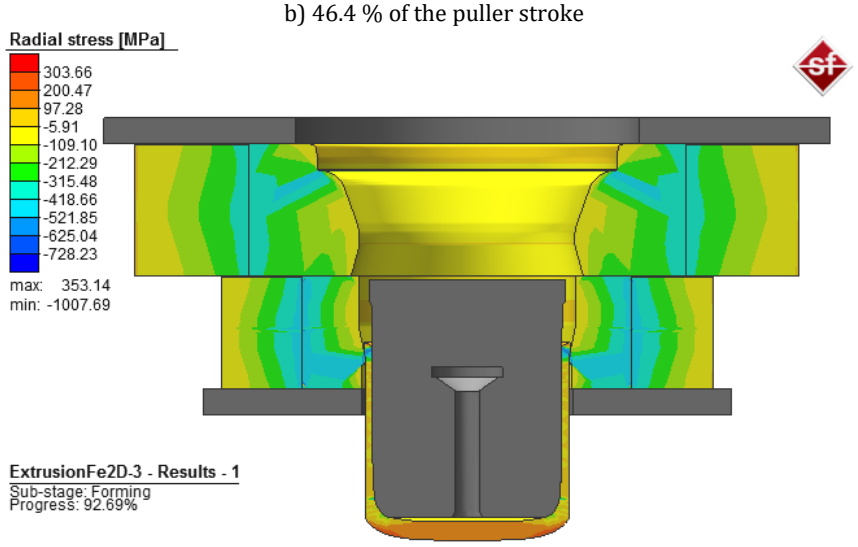

c) 92.7 % of the puller stroke

Fig. 12 Radial stress distributions in the workpiece and tools during coupled simulation of the deep drawing process

The second characteristic phase of the process (46.4 % of the stroke, Fig. 12b) includes the moment immediately before the exit of the workpiece from the calibrating zone of the upper die. It is noted that the maximum compressive radial stresses of -752 MPa are in the deformation zone of the workpiece at the very top, and that the upper part of the matrix along the tractrix curve is almost entirely relaxed. On the other hand, there is a decrease in tensile radial stresses at the bottom of the piece up to 178 MPa. In addition to the change in the shape of the workpiece, there is a small decrease in the thickness of the vessel wall.

In the last third selected phase of the process (92.7 % of the stroke), when the top of the workpiece is in contact with the calibrating zone of the lower die, maximum radial compressive stresses at the top of the vessel wall (-728 MPa) occur again. In contrast to passing material through the upper die, when the deep drawing process takes place, ironing is performed here, so the deformation of the workpiece in wall thickness is significant. This is transferred to the calibrating part of the die, but there is no large drop in compressive radial stresses (they amount to -520 MPa) because the ironing forces act differently on the die in the radial direction. There are no critical tensile stresses in the lower die and ring. However, the tensile radial stresses at the bottom of the vessel increased up to 300 MPa.

In order to more deeply analyse the thermo-mechanical processes in the numerical model of the deep drawing process, and compare them with industrial temperature measurements using infrared thermography, apart from the determination of the stresses in the workpiece and the tools, it is necessary to analyse the numerically estimated temperature fields.

Fig. 13a shows the temperature fields in the upper die obtained by the infrared thermal imager immediately after the process. For comparison, Fig. 13b shows the distribution of temperature fields obtained by FE numerical simulation. The contact friction between the tool and the workpiece, as well as the plastic deformation of the workpiece affected the temperature increase in the workpiece and the transfer of part of the temperature to the tools. The development of elevated temperatures in the upper die occurs in the output path of the tractrix curve in the range from 30°C to 77.1°C, with the maximum temperature being registered in the die calibration zone. The numerically estimated temperature field has a good coincidence as the maximum temperature of 77.9°C occurs on the same part of the die surface, and the range of the temperature field starts from 30°C. The advantage of the numerical simulation is that the temperature fields are calculated for the entire volume of the die, so the temperature fields can be analysed in any section and at any position, as opposed to physical measurements.

The measured temperatures in the lower die immediately after the process are shown in Fig. 14a, and the comparative distribution of the numerically estimated temperature fields is given in Fig. 14b. By analysing the temperatures on the lower die, it is noticed that there was a development of slightly higher temperatures in the range from 30°C to 90°C and a wider temperature field along the depth of the die, in the calibration zone where contact friction has the greatest influence. The reason for this is a longer contact with the workpiece, since the entire length of the vessel wall was in contact with this die during the ironing process. This was also confirmed by numerical simulation with the same area of elevated temperatures, with the fact that the maximum estimated temperature is slightly higher and amounts to 91.9°C.

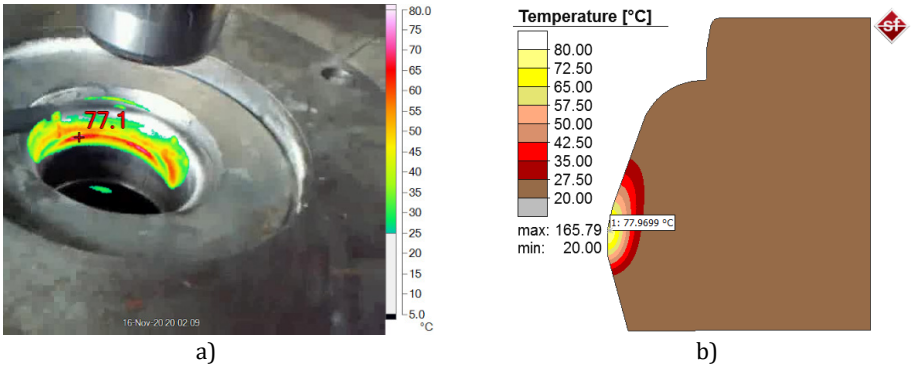

a) b)

Fig. 13 Comparison of the measured temperatures in the upper die (a) and numerically estimated (b)

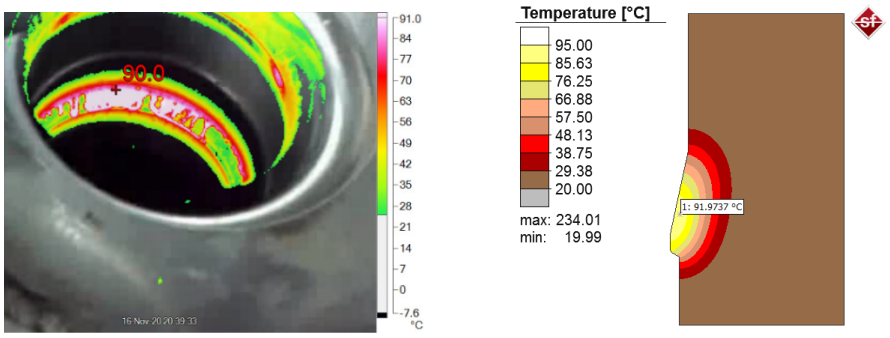

a) b)

Fig. 14 Comparison of the measured temperatures in the lower die (a) and numerically estimated (b)

Based on the analysed temperature fields, it can be concluded that the tool temperature values are relatively small. However, it must be emphasized that the simulation includes the deep drawing process of one workpiece, which means that it is expected that, during the longer exploitation of the tool, it will heat up more. Therefore, it is necessary to apply a cooling agent, in order to prevent overheating of the tool, which can lead to a change in the characteristics of the material, the appearance of temperature cracks and a short tool life.

Immediately after removing the workpiece from the tool in the industrial process, the temperatures were measured in the same way as for the tool. Arbitrary points on the thermal image were selected, as shown in Fig. 15a, in order to compare the values with the numerical temperature fields in the workpiece, shown in Fig. 15b. The legend of the industrial temperature measurements shows temperatures up to a maximum of 240°C, while the legend of the numerical model shows a value up to 233°C. In similar referent points, there is a satisfactory match between the measured and estimated temperatures in the workpiece. In the zone near the top of the vessel, the measured temperature was 182.1°C, and the numerically estimated temperature was 183.2°C. The lowest temperature values were registered and evaluated at the bottom of the vessel and range from 20°C to 45°C, because there was the least plastic deformation and there was no contact with the tool and thus no influence of contact friction.

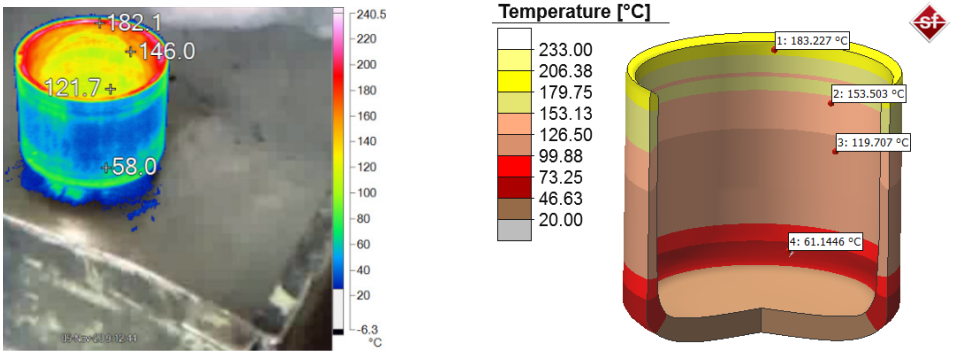

a) b)

Fig. 15 Comparison of the measured temperatures in the workpiece (a) and numerically estimated (b)

5. Conclusion

Deep drawing of thick sheets using tractrix die is a widely used technology in large-scale industrial production for the initial operations of obtaining special vessels, which require a significant difference in the thickness of the bottom and vessel walls, as well as special mechanical properties of the material in the characteristic sections. Reliable technology cannot be developed only through industrial trials, so the application of an experimental-numerical approach is more than necessary.

The aim of this study was to develop, through this approach, a reliable numerical thermo-mechanical model of the process for obtaining a silicon brass vessel in successive deep drawing and

ironing operations. It is known that the forming of thick sheets, as bulk deformation, is accompanied by an increase in temperature in the workpiece and transfer to the tools, so a comparative analysis of measured and numerically estimated temperatures in the workpiece and tools was used to validate the numerical model based on the finite element method.

The reliability of the numerical model is conditioned by high-quality input data for a set of FE simulations, which refer to models of material behaviour, contact friction and thermodynamic processes. The selection of adequate finite elements for the workpiece and deformable tools with constitutive relations that correspond to the physics of the process, then the parameters of the FE analysis and the conditions of automatic mesh generation and remeshing are crucial for precise and convergent numerical solutions. The paper provides a detailed description of the above-mentioned requirements, among other things, through the results of experimental testing of silicon brass material as well as temperature measurements before and after the deep drawing industrial process using an infrared thermal imager.

The numerical model of the process included the assembly phase of the upper and lower dies with reinforcing rings with an overlap in order to prestress and protect the dies. Adequate selection of overlaps and realised prestressing of the die is of essential importance for the accuracy of the parts, the reduction of the total tensile radial stresses, the dynamic cyclic loading of the die and its lifetime. The present study showed that identical overlaps cannot be applied in the upper and lower dies, so through repeated simulation with a changed value of the overlap of 1.3 mm, optimal prestresses were obtained.

Stress and temperature fields were analysed in the combined FE analysis of deep drawing and ironing processes with deformable prestressed tools. Numerical simulations, which are mostly performed with rigid tools, with or without the heat transfer option, do not provide a realistic numerical model of the industrial process. Therefore, the study established an expensive and time-consuming coupled FE numerical thermo-mechanical model through simultaneous plastic deformation of the workpiece, elastic deformation of the tools, heat generation due to plastic deformation and contact friction, heat loss due to transfer to tools and emissions to the environment. A comparative analysis of the temperature fields obtained by industrial measurements and numerical simulations showed a good agreement, thus validating the numerical model.

The establishment of a reliable and precise numerical model is the basis for investigating the influence of process parameters on other output indicators (strains, strain rates, forming load) and for making the desired modifications to the optimization of industrial technology. Temperature fields under other processing conditions and their influence on microstructure changes can be investigated with appropriate input data describing phase transformations in the material, which is the subject of future research using an integrated experimental-numerical approach.

Acknowledgement

The part of this research is supported by the Ministry of Science, Technological Development and Innovation, Republic of Serbia, Grant TR34002 and Grant TR32036, as well as Erasmus Grant 2020-1-ES01-KA203-081978

References

[1] Park, G., Park, R., Kwak, H., Kim, C. (2021). Design of a combined redrawing-ironing process to manufacture a CNG pressure vessel liner, *Applied Sciences,* Vol. 11, No. 18, Article No. 8295, doi: 10.3390/app11188295.

[2] Pernis, R., Barényi, I., Kasala, J., Ličková, M. (2015). Evaluation of limiting drawing ration (LDR) in deep drawing process, *Acta Metallurgica Slovaca*, Vol. 21, No. 4, 258-268, doi: 10.12776/ams.v21i4.642.

[3] Kesharwani, R.K., Basak, S., Panda, S.K., Pal, S.K. (2017). Improvement in limiting drawing ratio of aluminum tailored friction stir welded blanks using modified conical tractrix die, *Journal of Manufacturing Processes*, Vol. 28, Part 1, 137-155, doi: 10.1016/j.jmapro.2017.06.002.

[4] Loganathan, C., Narayanasamy, R. (2005). Effect of mechanical properties on the wrinkling behaviour of three different commercially pure aluminium grades when drawn through conical and tractrix dies, *Materials Science and Engineering: A,* Vol. 406, No. 1-2, 229-253, doi: 10.1016/j.msea.2005.06.037.

[5] Park, G.-Y., Kwak, H.-S., Jang, H.-S., Kim, C. (2022). Deep drawing process using a tractrix die for manufacturing liners for a CNG high-pressure vessel (Type II), *Chinese Journal of Mechanical Engineering*, Vol. 35, No. 15, 1-12, doi: 10.1186/s10033-022-00681-9.

[6] Reddy, A.C.S., Rajesham, S., Reddy, P.R. (2015). Experimental and simulation study on the warm deep drawing of AZ31 alloy, *Advances in Production Engineering & Management*, Vol. 10, No. 3, 153-161, doi: 10.14743/apem2015.3.199.
[7] Mandic, V. (2012). *Physical and numerical modelling of metal forming processes (in Serbian),* Faculty of Mechanical Engineering, Kragujevac, Serbia.
[8] Hrnjica, B., Behrem, Š. (2022), A new multi-objective optimization approach for process parameters optimization during numerical simulation of quenching steel parts, *Advances in Production Engineering & Management*, Vol. 17, No. 1, 16-32, doi: 10.14743/apem2022.1.418.
[9] Mandić, V., Ćosić, P. (2011). Integrated product and process development in collaborative virtual engineering environment, *Tehnički Vjesnik – Technical Gazette,* Vol. 18, No. 3, 369-378.
[10] Gusel, L., Boskovic, V., Domitner, J., Ficko, M., Brezocnik, M. (2018). Genetic programming method for modelling of cup height in deep drawing process, *Advances in Production Engineering & Management*, Vol. 13, No. 3, 358-365, doi: 10.14743/apem2018.3.296.
[11] Adamovic, D., Mandic, V., Jurkovic, Z., Grizelj, B., Stefanovic, M., Marinkovic, T., Aleksandrovic, S. (2010). An experimental modelling and numerical FE analysis of steel-strip ironing process, *Tehnički Vjesnik – Technical Gazette,* Vol. 17, No. 4, 435-444.
[12] Elplacy, F., Samuel, M. Mostafa, R. (2022), Modelling and simulation of hot direct extrusion process for optimal product characteristics: Single and multi-response optimization approach, *Advances in Production Engineering & Management*, Vol. 17, No. 1, 33-44, doi: 10.14743/apem2022.1.419.
[13] Tomáš, M., Evin, E., Kepič, J., Hudák, J. (2019). Physical modelling and numerical simulation of the deep drawing process of a box-shaped product focused on material limits determination, *Metals*, Vol. 9, No. 10, 1058-1074, doi: 10.3390/met9101058.
[14] Volk, M., Nardin, B., Dolsak, B. (2014). Determining the optimal area-dependent blank holder forces in deep drawing using the response surface method, *Advances in Production Engineering & Management*, Vol. 9, No. 2, 71-82, doi: 10.14743/apem2014.2.177.
[15] Musafija, B. (1979). *Metal forming by plastic deformation*, Svetlost, Sarajevo, Bosnia and Herzegovina.
[16] Romhanji, E., Milenković, V., Drobnjak, D. (1992). The grain size and alloying influence on the strain hardening of polyerystalline α-brasses, *International Journal of Materials Research*, Vol. 83, No. 2, 110-114, doi: 10.1515/ijmr-1992-830208.
[17] Hexagon. HxGN virtual manufacturing, from *https://www.simufact.com/simufactforming-forming-simulation.html*, accessed November 25, 2023.
[18] Popović, M., Mandić, V., Delić, M., Pavićević, V. (2021). Experimental-numerical analysis of hot forging process with monitoring of heat effects, In: Karabegović, I. (ed.), *New technologies, development and application IV, NT 2021, Lecture notes in networks and systems*, Springer, Cham, Switzerland, 341-349, doi: 10.1007/978-3-030-75275-0_38.
[19] Hou, F., Zhang, Y., Zhou, Y., Zhang, M., Lv, V., Wu, J. (2022). Review on infrared imaging technology, *Sustainability,* Vol. 14, No. 18, Article No. 11161, doi: 10.3390/su141811161.
[20] Usamentiaga, R., Venegas, P., Guerediaga, J., Vega, L., Molleda, J., Bulnes, F. (2014). Infrared thermography for temperature measurement and non-destructive testing, *Sensors*, Vol. 14, No. 7, 12305-12348, doi: 10.3390/ s140712305.
[21] Fluke. Ti200, Ti300, Ti400, Thermal imagers, Users manual, from *https://www.fluke-direct.com/pdfs/cache/www.fluke-direct.com/ti200-60hz/manual/ti200-60hz-manual.pdf*, accessed December 15, 2023.